Dislocation dynamics simulations of the relaxation of intrinsic stress in thin films

Can Ayas, Erik van Der Giessen

Dislocation dynamics simulations of the relaxation of intrinsic stress in thin films

Journal:	*Philosophical Magazine & Philosophical Magazine Letters*
Manuscript ID:	TPHM-07-Dec-0356.R1
Journal Selection:	Philosophical Magazine
Date Submitted by the Author:	07-Feb-2008
Complete List of Authors:	Ayas, Can; University of Groningen, Zernike Institute of Advanced Materials van der Giessen, Erik; University of Groningen, Zernike Institute of Advanced Materials
Keywords:	dislocation dynamics, stress relaxation, thin films
Keywords (user supplied):	dislocation dynamics, stress relaxation, thin films
Note: The following files were submitted by the author for peer review, but cannot be converted to PDF. You must view these files (e.g. movies) online.	
revision.tex	

Philosophical Magazine,
Vol. 00, No. 00, DD Month 200x, 1–12

Dislocation dynamics simulations of the relaxation of intrinsic stress in thin films

C. Ayas & E. Van der Giessen*

Zernike Institude of Advanced Materials, Nyenborgh 4, 9747 AG Groningen, The Netherlands.

(Received 00 Month 200x; in final form 00 Month 200x)

The relaxation of compressive intrinsic stress for a film/substrate system is modeled with discrete dislocation dynamics (DDD). Compressive stress is arising due to the diffusion of extra material into the grain boundaries during deposition. Dislocation nucleation and motion relax the stress in the thin film. The effect of microstructure on the process is found to be two-fold. As the grains get finer, the initial compressive stress becomes higher and more homogeneous, while impenetrable grain boundaries also cause higher hardening. The two effects seem to balance out when there are few sources available for dislocation nucleation. When the density of sources is high, relaxation behavior seems to be less affected by microstructure since both effects get weaker when the limit of continuum behavior is approached.

1 Introduction

Thin metallic films are routinely used at (sub)micrometer scales in applications such as integrated microelectronic circuits and micro-electro-mechanical systems (MEMS). Although these films are not primarily designed for load bearing applications, mechanical properties of small scale devices are of importance for reliability, and hence understanding them is insightful for sustainable design.

In this study we focus on the intrinsic growth stresses that are due to the non-equilibrium nature of film synthesis techniques. The evolution of the stress state has been experimentally studied by in situ monitoring of the film average stress during deposition, e.g. [1]. Abermann [2] distinguished two types of characteristic stress evolution in polycrystalline thin films. Films with relatively low melting temperatures are susceptible to appreciable diffusion at deposition temperature and usually end up building up an average compressive stress. On the other hand, tensile stresses are observed for high melting point materials.

The origin of both classes of behavior resides in the Volmer–Weber growth mechanism of polycrystalline films. As long as the binding interaction between film atoms is stronger than the binding interaction between film and substrate atoms, film growth starts out by island formation. The evolution of stress in the film then reveals three distinct stages. During the first stage, small islands on the substrate nucleate and the film is in compression as a consequence of surface stress. As islands grow, the magnitude of the compressive stress decreases. The second stage starts when independent islands have grown so much that they touch each other. It then is energetically favorable to transform two free surfaces into one grain boundary. The film grains deform slightly to accommodate this zipping process as long as the elastic strain energy gained is less than the energy consumption for grain boundary formation. When coalescence of the islands into grains is complete, the peak tensile stress is attained, [3, 4]. The third stage of growth is still not completely understood and a number of mechanisms have been proposed in the literature, e.g. [5–9]. According to Chason et al. [9] adatoms are continuously arriving at the film surface during deposition where they create a supersaturated adatom population. Accordingly, a chemical potential difference between the free surface and the uppermost part of the grain boundary builds up. This induces a chemical potential gradient, which drives a flux of atoms into the film along the grain boundaries. Diffusion of extra material relaxes the tensile stress and depending on the process parameters different tensile and, even, compressive stress levels can be attained [9]. The stress magnitude depends on the competition between film growth and diffusion. If the growth rate of film is low, or equivalently when the deposition temperature is high,

*Corresponding author. Email: E.van.der.Giessen@rug.nl

Philosophical Magazine
ISSN 1478-6435 print/ISSN 1478-6443 online © 200x Taylor & Francis
http://www.tandf.co.uk/journals
DOI: 10.1080/1478643YYxxxxxxxx

significant diffusion can occur leading to a pronounced compressive stress, while for fast growth, even some tensile stress may be frozen-in in the film. It is also important to note once again that the driving force for diffusion is chemical potential difference due to supersaturated adatom population at the free surface. Hence, even when the tensile stress due to former island coalescence stage is totally relaxed to zero, diffusion may continue because the ongoing deposition process still pushes gas atoms near the film's advancing front, thus supplying a chemical potential gradient. Actually when there is no constraint for diffusion, intrinsic compressive stress continues to build up to a level decided by adatom supersaturation. Grain boundary diffusion, being much slower than surface diffusion, is the rate-controlling process and therefore governs stress evolution. A mechanistic model describing these observations has been given by Gudurui*et al.* [10]. The third stage of stress evolution is absent in films with a high melting temperature because diffusion is too slow.

Relaxation of the intrinsic compressive stress may occur by dislocation plasticity, debonding of the film from the substrate or by reverse diffusion caused by reversal of the chemical potential gradient after deposition halts. The various relaxation mechanisms can be triggered already during film deposition, but in order to gain some basic insight, in this paper we decouple growth and diffusion from dislocation plasticity, and focus solely on the latter.

We consider a thin metal film on a substrate just after deposition, but still at the deposition temperature. During deposition, diffusion of adatoms is assumed to have created a compressive stress above the yield strength of the film material. The stress will relax by plasticity, eventually leaving some residual stress. It bears emphasis that we do not take into account the coupling between film growth, diffusion and plasticity, but look solely into plastic flow in the initially compressed film. Plastic relaxation is described using discrete dislocation plasticity, where individual dislocations can be nucleated and glide on discrete slip planes. The dislocations themselves are treated as singularities in an elastic background, and superposition is used to satisfy the boundary conditions, [11]. This approach has shown previously to be able to pick up size effects in films with thicknesses on the order of fractions to several micrometers, e.g. [12–14]. The objective of the present paper is to study the effect of microstructure, in particular grain size and density of dislocation sources, on the propensity of relaxation of intrinsic compressive stress.

2 Method

We consider the plane-strain problem of a thin film of infinite width that is perfectly bonded to a very thick elastic substrate, as illustrated in figure 1. The film has thickness h and comprises columnar grains of width d, each containing three slip systems. Obviously, in real materials, the orientation of the grains varies, but here we will assume all grains to have the same orientation. This simplification is motivated by the finding in [15] that the role of grain boundaries as obstacles for dislocation motion is more important in controlling the Hall–Petch grain size effect than lattice mismatch. Thus, the slip planes are oriented at mutual angles of 60°, with one of them being parallel to the film–substrate interface. This mimics, in two dimensions, an FCC crystal with (001) coinciding with the interface and the (110) plane being the plane of consideration. As shown by Rice [16] this orientation allows for plane strain deformations by virtue of the symmetry of the $\langle 110 \rangle$ slip directions on the $\{111\}$ planes.

The infinitely wide film is modeled by considering a plane-strain, periodic cell of width w in x_1 direction. Periodic boundary conditions on the cell edges (denoted by π in figure 1) ensure displacement and traction continuity along the sides,

$$u_i(0, x_2) = u_i(w, x_2), \quad \sigma_{1i}(0, x_2) = \sigma_{1i}(w, x_2), \quad i = 1, 2\,. \tag{1}$$

The substrate is considered to be elastic, while plastic flow in the film is modeled by the dynamics of discrete dislocations, treated as line singularities in the otherwise elastic medium. A statistically meaningful sample of the film is obtained when the computational cell contains several grains; when the latter is not the case, multiple realizations of the computational cell are needed.

Two sets of discrete dislocation computations are carried out. The main simulation is that of the relaxation of the initial stress state induced by the material inserted into the grain boundary during deposition.

The thickness (or opening) of the grain boundary is determined by an independent calculation, described subsequently, and serves as the initial condition for the dislocation plasticity simulation. The second type of computation is performed to capture the hardening behavior of the film material itself, i.e. in the absence of intrinsic stress. In the latter case, straining of the film is imposed by making use of the thermal mismatch between film and substrate, which upon cooling induces a tensile stress in the film when the film's expansion coefficient is larger than that of the substrate. The thermal stress increases with decreasing temperature, and plasticity is triggered when the stress level is high enough to nucleate and move dislocations. This kind of computation is similar to that reported by Nicola *et al.* [13] and serves here merely to substantiate the interpretation of the intrinsic stress relaxation results.

2.1 *Initial compressive stress*

As mentioned before, a compressive stress can develop in the film by diffusion of adatoms into the grain boundary when the growth rate is relatively low. According to Gao *et al.* [17], the grain boundary opening due to diffusion of extra material can be approximated by the opening displacement of a mode I crack. This leads to the distribution of grain boundary separation δ being given by

$$\delta(x_2) = \delta(h)\sqrt{1-(1-x_2/h)^2}\,. \tag{2}$$

The prefactor $\delta(h)$ is a measure of the average induced stress in the film. Its value, defining the total amount of material diffused along the grain boundary, is determined by the deposition process, but will be considered an input variable for the model here.

For convenience within a framework for discrete dislocations, the local boundary opening according to equation (2) is discretized by distributing edge dislocations along each grain boundary, whose Burgers vector is parallel to the film substrate interface.[1] They are introduced in the form of dipoles to ensure proper orientation of the displacement discontinuity so as to represent the inserted material. The negative ends of the dipoles reside at the free surface while the positive parts are placed along the boundary with a separation between them, Δl. A single dipole with Burgers vector b at $x_2 = y$ therefore produces an opening $\delta(x_2) = bH(x_2 - y)$ along $x_2 < h$ (neglecting core effects; $H(x)$ is the Heaviside step function: $H = 1$ for $x > 0$, $H = 0$ elsewhere). As a consequence, the separation at any point on the boundary is determined by all the grain boundary dislocations that are below that point. Equal dislocations at a regular spacing produce a linear wedge opening of the grain boundary; a nonlinear variation of the opening is obtained by varying the magnitude $b^{(I)}$ of the misfit dislocations (or the spacing, but we here choose to keep this constant and equal to the slip plane spacing). With the n dislocations positioned at $x_2 = X_2^{(I)} := I\Delta l$, the (discretized) opening becomes

$$\delta(x_2) = \sum_{I=1}^{n} b^{(I)} H(x_2 - X_2^{(I)}) \tag{3}$$

The full displacement field, along with the induced strain and stress fields, is computed by means of the superposition method [11] in order that the boundary conditions are met (as will be summarized in some detail in the next subsection).

As an example, a film with $h = 0.5\ \mu$m having $n = 20$ dislocations along the grain boundary (so that $\Delta l = 0.025\ \mu$m) is taken here to explain the procedure. The grain boundary opening calculated from equation (2) is shown with the solid curve in figure 2. Here we have chosen $\delta(h) = 2.6\,$nm; this corresponds to an initial stress state with an average film stress of -75.7 MPa for which significant relaxation will occur for the chosen material parameters. The values of $b^{(I)}$ are computed sequentially for $I = 1$ to n by application of equation (3) at the nodes of the finite element mesh. The resulting discretized opening profile

[1] For simplicity, we refer to the dislocations describing the grain boundary opening as "grain boundary dislocations", even tough there is no orientation mismatch between grains.

shown by the dashed curve provides a good approximation. The corresponding stress and deformation fields are shown in figure 3.

2.2 *Discrete dislocation plasticity*

Not only the grain boundary dislocations but also the dislocations that can relax the resulting stresses by glide are of edge character; the key distinction is that the latter dislocations live on the three slip systems indicated in figure 1. In either case, we adopt the approach in [11] and decompose the dislocation fields into a singular long-range field, denoted by $(\tilde{})$, and a non-singular image field $(\hat{})$ to correct for the boundary and periodicity conditions. Hence, for example for stress,

$$\sigma_{ij} = \hat{\sigma}_{ij} + \sum_I \tilde{\sigma}_{ij}^{(I)}, \tag{4}$$

with I being an index for a dislocation. For the $(\tilde{})$-fields we here make use of the closed-form expressions for a periodic array of dislocations in half-infinite space given in [18]. By construction, these fields already satisfy periodicity conditions at the sides and the traction-free conditions at the top surface of the film. The $(\hat{})$-fields serve to satisfy the boundary conditions at the bottom of the substrate: $u_2 = 0$ and $\sigma_{21} = 0$. These nonsingular, image fields are obtained by the finite element method, using a quadrilateral mesh (as can be seen in figure 3b). Both fields are computed at each time increment, once the dislocation structure is updated for that step. While the long-range interactions between dislocations are captured by their elastic fields, the interactions at small distances are described by a set of constituve rules.

Glide dislocations get nucleated from two-dimensional Frank-Read sources that are positioned randomly on slip planes (spaced, in the present computations, at $100b$ with a magnitude $b = 0.25$nm of the Burgers vector). These sources generate a dipole when the resolved shear stress at the source exceeds the strength τ_{nuc} for a sufficiently long time (here, $t_{\text{nuc}} = 10$ns). The source strengths are randomly selected from a Gaussian distribution with a mean strength $\bar{\tau}_{\text{nuc}} = 25$MPa and a standard deviation of 5MPa. The sign of the generated dipole depends on the sign of the resolved shear stress τ. At the instant of nucleation, the two ends of the dipole are initially separated at a distance L_{nuc}, given by

$$L_{\text{nuc}} = \frac{\mu}{2\pi(1-\nu)} \frac{b}{\tau_{\text{nuc}}} \tag{5}$$

so that the attractive interaction between them does not make the dipole collapse right away.

The motion of the glide dislocations is governed by the Peach-Koehler force, i.e. the potential energy change of the system for an infinitesimal change in the position of the dislocation of interest. The component of that force in the direction of slip is given by [11]

$$f^{(I)} = m_i^{(I)} (\hat{\sigma}_{ij} + \sum_{J \neq I} \tilde{\sigma}_{ij}^{(J)}) b_j^{(I)} \tag{6}$$

where $m_i^{(I)}$ is the unit normal to the slip system on which the dislocation I with Burgers vector $b_j^{(I)}$ resides. The motion of dislocations is taken to be drag controlled with a drag coefficient of $B = 10^4$Pa s, so that the glide velocity is given by $v^I = f^I/B$.

Dislocations with opposite sign get annihilated if they come closer than $6b$ to each other. In the present computations, there are no obstacles to dislocation motion inside the grains, but the film–substrate interface and the grain boundaries are assumed to be impenetrable to dislocations.

3 Results and Discussion

We consider thin films with varying grain sizes d, but with the same thickness of $h = 0.5\,\mu$m. Elasticity in both film and substrate is linear isotropic; Young's modulus is taken to be $E = 70$GPa, while Poisson's ratio is $\nu = 0.33$ (it is known from [12] that the effect of elastic mismatch is negligible). The thermal expansion coefficients of film and substrate are $\alpha_{\rm f} = 23.2\times10^{-6}$/K and $\alpha_{\rm s} = 4.2\times10^{-6}$/K, respectively. In the cooling simulations, a cooling rate of 40×10^{6}K/sec is adopted. The time step used for cooling simulations is 0.05ns, while a smaller time increment of 0.005ns was found necessary to resolve the dislocation movement during relaxation simulations.

3.1 *Relaxation: concerted action of dislocation generation and hardening*

Relaxation simulations start from an initial compressive state of stress governed by the opening distribution equation (2). As mentioned previously, we regard the maximum grain boundary opening $\delta(h)$ to be an input parameter. Its value of 2.6 nm in films with $d = 2\,\mu$m gives rise to the initial stress state shown in figure 3a, with a film average value of $\langle\sigma_{11}(0)\rangle = -75.7$ MPa.

The relaxation behavior of thin films with $d = 2\,\mu$m for different source densities is presented in figure 4a in terms of the evolution of the film average stress $\langle\sigma_{11}\rangle$ normalized with the initial film average stress $\langle\sigma_{11}(0)\rangle$. Time is normalized by the nucleation time. Each curve shown is an average of five different source distributions and the error bars denote the standard deviation of the data. A source density of $\rho_{\rm nuc} = 60\,\mu{\rm m}^{-2}$ is the central case in this parameter study (as in [13]), but we also consider a low density of $30\,\mu{\rm m}^{-2}$ and a higher one, $\rho_{\rm nuc} = 240\,\mu{\rm m}^{-2}$.

For all source densities analyzed, the stress relaxation curves have the same characteristic shape. Relaxation starts after an incubation period equal to the nucleation time, after which nucleation and motion of the glide dislocations take place. As seen in figure 4a, both the rate of decay and the maximum relaxation achievable depend on the source density. The total reduction of stress is the manifestation of the collective motion of all glide dislocations. Under the influence of the predominant σ_{11} stress state (with Schmid factor $\frac{1}{2}\sin 2\phi$), the positive dislocations on slip planes with $\phi = 60^\circ$ and the negative ones on the 120° slip planes tend to move towards the free surface; when they exit the crystal they leave a surface step. The opposite-signed dislocations tend to pile-up against the film/substrate interface or the grain boundaries were they are blocked. It is this interplay between nucleation, glide and the development of back stresses caused by pile-ups that governs the characteristic decay.

Because relaxation proceeds with plastic deformation, material hardening also comes into the picture. Hardening in the present model is due to the hindrance of dislocation motion by (i) dislocations piling-up against a grain boundary or the film/substrate interface, and (ii) 'collision' and 'locking' with a dislocation on another slip plane. This hardening behavior is studied separately in cooling simulations of the same films (but without initial stress). According to figure 4b, hardening is nearly linear with imposed strain and decreases with increasing source density (see also [12, 13]). The latter is a partial explanation for the observation in figure 4a that the final residual stress after relaxation is higher (in absolute value) for lower source densities.

The relative contributions to relaxation by nucleation and glide can be better understood by investigating the evolution of dislocation density, as shown in figure 5. In films with relatively coarse grains ($d = 2\,\mu$m; solid curves), plasticity seems to be glide dominated. The dislocations that are needed for relaxation are generated in the early stages right after $t = t_{\rm nuc}$; their density only decreases with time as dislocations escape from the crystal through the free surface. Note that for the highest source density of $\rho_{\rm nuc} = 240\,\mu{\rm m}^{-2}$, many dislocations nucleated at $t = t_{\rm nuc}$ were not sustainable and annihilated again. This sharp peak seen in figure 5 is responsible for the sharp stress drop in figure 4a for $\rho_{\rm nuc} = 240\,\mu{\rm m}^{-2}$.

As the source density increases, relaxation is more efficient in the sense of a lower (in absolute value) final residual stress that can no longer be relaxed. From figure 4a one finds that the average residual stress varies from -24.4 MPa for the lowest source density to -10.4 MPa when $\rho_{\rm nuc} = 240\,\mu{\rm m}^{-2}$. One reason for this sensitivity to source density is that the likelihood of weak sources is higher when the source density is larger, but the main reason is the increased probability of finding a source in a favorable condition

to nucleate. Taking into account the Schmid factor, all residual stresses from figure 4a correspond to a resolved shear stress on the inclined slip planes is smaller than the strength of the weakest source that happens to be present. Having infinitely many sources would conceptually be approaching a continuum theory, where (implicitly) sufficiently many sources are available whenever and wherever they are needed. Stress relaxation in continuum theory would therefore occur instantly (aside from rate effects), and would depend only on the yield strength. However, even in a hypothetical infinite-source discrete dislocation framework still some time is spent on nucleation.

3.2 *Grain size effect*

Hardening in thin films depends on grain size [13]; what is the effect of grain size on the relaxation behavior of intrinsic stress? This cannot be addressed by solely changing the value of d, but also requires consideration of the initial compressive stress, or in other words the value of the maximum grain boundary opening $\delta(h)$ in equation (2). As described in detail by Guduru *et* al. [10], the diffusion of material into a grain boundary during deposition is governed by the local (compressive) stress along the boundary and by the injection rate at the growing surface, assuming that grain boundary diffusion is the rate-limiting step. Although the solution for multiple grain boundaries is not yet available, we can make a number of simple observations. First of all, we point out that the compressive stress field induced by the grain boundary opening decays almost exponentially with distance from the grain boundary (exponential decay is exact for a perfect tilt wall comprising equal dislocations; it is not exact for the variations in Burgers vector seen in figure 2, but it is fairly close to that). This means that, when the grain size is much larger than the film thickness, the normal stress along a particular grain boundary is not affected significantly by diffusion on the neighboring boundary. Hence, one would expect $\delta(h)$ to be independent of grain size for coarse grained microstructures. On the other hand, when d is very small and the boundaries communicate with each other almost directly, diffusion at a neighboring grain would restrict the diffusion at the grain boundary of interest. In this case it is more likely that $\delta(h)/d$ is constant where, the total diffused material is distributed equally among all boundaries.

Awaiting a quantitative solution, we here consider the two extreme cases. First, the opening per grain boundary is kept constant (i.e. $\delta(h)$ is independent of d); this leads to films having a higher initial stress as the grains get finer. The other extreme case is that $\delta(h)/d$ is constant, which implies the same average initial stress irrespective of grain size.

3.2.1 ***Identical grain boundary opening.*** Figure 6a presents results for a grain size of $d = 0.5\ \mu$m. Compared to the results for $d = 2\ \mu$m in figure 4a, the finer microstructure is seen to induce important changes in the relaxation curves. Considering first the films with $\rho_{\text{nuc}} = 30\mu\text{m}^{-2}$, we see that the relaxation curve is less smooth than for $d = 2\ \mu$m, figure 4a. There are two reasons for this. Firstly, as the initial compressive stress increases with decreasing grain size, there is a notable difference in the mechanism of relaxation, viz. it becomes more nucleation controlled. The initial resolved stresses are so high that the first dipoles of nucleated dislocations glide apart and reach their final positions very rapidly, even within the nucleation time. After $2t_{\text{nuc}}$, new dislocations are nucleated, which again move rapidly and relax the stress down to a lower plateau. This process repeats every nucleation cycle, with the amount of relaxation per cycle gradually reducing until a steady stress state is achieved. This phenomenon can also be seen from the evolution of the dislocation density, shown, for even finer grains with $d = 0.25\ \mu$m, in figure 5. The second striking difference is that the dislocation motion is more restricted due to the increased amount of impenetrable grain boundary length per unit area. This couples back to the aforementioned nucleation domination, since reduced dislocation motion calls for the creation of dislocations in order for plasticity to be sustained. As a consequence, relaxation completes but the residual stress in $d = 0.5\ \mu$m films with $\rho_{\text{nuc}} = 30\ \mu\text{m}^{-2}$ is almost three times higher than that when $d = 2\ \mu$m. The characteristic time scale for relaxation does not appear to be very sensitive to grain size.

In a similar fashion, figure 6b reveals the effect of grain size on the behavior during thermal relaxation of the same films. As was seen in figure 4b for $d = 2\ \mu$m, a higher source density lowers the amount

of hardening. When comparing figure 6b to figure 4b, we observe that hardening is slightly stronger in fine grained films that have a high density of sources ($\rho_{\text{nuc}} = 240\ \mu\text{m}^{-2}$), but that hardening is increased dramatically at low source density. In the latter case, the back stresses created by piled-up dislocations tend to shut off sources (see [13] for a more in-depth discussion). This suppression of source activity is illustrated for relaxation calculations, by the distributions of the resolved shear stress on the three slip systems for a typical $\rho_{\text{nuc}} = 30\ \mu\text{m}^{-2}$ case but an even smaller grain size of $d = 0.25\ \mu\text{m}$ in figure 7. The shear stress at the sources is low due to the back stress arising from the dislocation pile-ups. Because of this, the shear component of the average residual stress resolved in the inclined slip planes is larger than the minimum source strength (contrary to the previous cases with $d = 2\ \mu\text{m}$); in fact, the residual stress is below the average source strength only for the highest source density. Figure 7 also reveals a few dislocations on horizontal glide planes, despite the fact that the nominal Schmid factor vanishes there; their nucleation has been caused by the stress field of dislocations on other systems.

As the source density increases for a fixed d, more relaxation occurs and therefore lower residual stress levels are observed. When we compare this trend in figure 4 with that in figure 6 it is observed that when the grains get finer, an increase in source density from $\rho_{\text{nuc}} = 30\ \mu\text{m}^{-2}$ to $240\ \mu\text{m}^{-2}$ lowers the residual stress by a factor of around three when $d = 0.5\ \mu\text{m}$ compared to only two when $d = 2\ \mu\text{m}$. The reason for this enhanced sensitivity is that hardening is more sensitive to source density for finer grains.

Finally, we compile the residual stresses predicted by the simulations (in Figs. 4a and 6a at $t/t_{\text{nuc}} = 10$) for various source densities and plot them as a function of grain size in figure 8a. When the source density is low, $\rho_{\text{nuc}} = 30\ \mu\text{m}^{-2}$, there appear to be two opposing effects that control the residual stress level. As the grain size decreases, the initial compressive stress, being the driving force for relaxation, increases as discussed above. On the other hand, when the grain size decreases, dislocation motion becomes more and more restricted. These two opposing effects balance at some intermediate point. When the source density increases and hardening weakens, the balance between the opposing effects is less pronounced ($\rho_{\text{nuc}} = 60\ \mu\text{m}^{-2}$). For the highest source density ($\rho_{\text{nuc}} = 240\ \mu\text{m}^{-2}$) considered, relaxation is nearly microstructure independent. The hardening behavior for the different cases can be seen in figure 8(b) where $\langle\sigma_{11}\rangle$ values at $T = 300K$ are compiled for all hardening simulations. Two important points should be noted. When the source density increases, hardening is weaker. Secondly there seems to be a correlation between grain size d and thickness of the film h. For all source densities, there seems to be practically no difference in terms of hardening between films with $d = 2\ \mu\text{m}$ and $d = 1\ \mu\text{m}$. Size effects in this range are probably controlled by the film thickness $h = 0.5\,\mu\text{m}$. Only after d becomes comparable with h it becomes the controlling parameter. Because plasticity at small scales is affected by stress states and microstructural variables through the scarcity of dislocations, relaxation of intrinsic stresses and resulting residual stresses are not independent of microstructural parameters.

It is noted that, although there is an a priori spacing between slip planes in the simulation, the spacing between active glide systems is controlled essentially by the distance between sources ($1/\sqrt{\rho_{\text{nuc}}}$ on average). While the former is chosen equal to $\Delta l = 0.025\ \mu\text{m}$, the actual source spacing varies from $0.06\ \mu\text{m}$ for the highest density $\rho_{\text{nuc}} = 240\ \mu\text{m}^{-2}$ to $0.18\ \mu\text{m}$ for $\rho_{\text{nuc}} = 30\ \mu\text{m}^{-2}$. Although grain boundary and glide dislocations play a different role, it is of interest to investigate the influence of the presumed spacing between dislocations in the grain boundaries. A smaller spacing will enable the grain boundary opening (cf. figure 2) to be more accurately mimicked, but figure 9 proves that the distance $\Delta l = 0.025\ \mu\text{m}$ used in all computations reported on here is small enough for the relaxation results to be independent of it.

3.2.2 ***Constant total amount of grain boundary material.*** When the relaxation simulations are carried out with a constant amount of grain boundary material in the film, i.e. $\delta(h)/d$ is constant, the grain size dependence of the driving force for relaxation is expected to fade; this would leave the relaxation behavior to be governed by the size dependence of hardening. However grain size still plays a role, by virtue of the inhomogeneity of the stress state for an array of dislocations. To illustrate this effect, figure 10 shows the resolved shear stress on the three slip systems before relaxation starts, for two different grain sizes. It is observed that the resolved shear stress on slip planes with $\phi = 0°$ is anyway rather low. Slip planes of this system are not very significant in the course of relaxation. However on the other two slip systems, where most of the dislocation activity occurs, there is a significant change in the resolved stress distributions

with grain size, eventhough the film averages are the same. When the grains are coarse, such as $d = 2\,\mu$m in figure 10a, there is a relatively large area along the film/substrate interface where τ is lower than $|\tau_{\rm nuc}|$ which means that this part of the film is not expected to be susceptible to nucleation, at least in the beginning. In the course of the relaxation process, dislocations pushed into this area may invoke some nucleation or there may be sources in the low stress area which have a significantly lower $\tau_{\rm nuc}$ than the average strength and therefore still able to nucleate. However, averaging over different realizations rules out these coincidental situations to be decisive. For finer grains (see figure 10b) the domain where τ is not high enough to trigger nucleation is significantly smaller. The inhomogeneity effect is likely to be effective when the source density is low, as it reduces the density of potentially active sources even further. However when the source density is high, there are still enough sources to effectively relax the initial stress. It should be noted that in the cooling calculations, where we consider the hardening behavior of different microstructures, the inhomogeneity effect is absent since the resolved shear stress arising from the thermal mismatch is homogenous through the film.

In order to see the overall relaxation trends when it assumed that the total amount of material injected in grain boundaries is independent of grain size, figure 11 presents the compilation of the relaxation simulation results. For a high source density of $\rho_{\rm nuc} = 240\,\mu{\rm m}^{-2}$ the amount of relaxation correlates with the hardening, and the inhomogeneity effect is not dominant (as expected). For grain sizes in the range 2–0.5μm , relaxation seems to be independent within the statistical scatter, just like the hardening behavior of the same film shown with the dotted line in figure 8(b). In films with $\rho_{\rm nuc} = 60\,\mu{\rm m}^{-2}$, hardening is stronger but exhibits the same grain size dependence (cf. figure 8(b)), and according to figure 11 the relaxation behavior also shows a similar trend as for $\rho_{\rm nuc} = 240\,\mu{\rm m}^{-2}$. This suggests that even for this source density, hardening is the dominant effect. However, for the lowest source density considered, $\rho_{\rm nuc} = 30\,\mu{\rm m}^{-2}$, the grain size dependence of relaxation reveals an additional effect. Although the hardening is even stronger than for the other source densities (see figure 8b), the inhomogeneity of the resolved shear stress act as an opposing effect and promotes more relaxation as grains becomes finer. For a grain size below $0.25\,\mu$m, the influence of stress inhomogeneity has saturated and hardening takes control of the size dependence again.

4 Conclusions

We have explored the relaxation of intrinsic growth stresses in thin films with columnar grains by dislocation plasticity. The initial compressive stress arising from the diffusion of adatoms into grain boundaries has been modeled by an array of dislocations along the grain boundary. Plastic relaxation of stress was incorporated by dislocation nucleation and glide. The grain size in films with a thickness of $0.5\,\mu$m has been varied between $0.25\,\mu$m and $2\,\mu$m. A parameter study with the density of dislocation sources in the range of 30–240 $\mu{\rm m}^{-2}$ revealed the following features:

- Dislocation plasticity relaxes the initial compressive stress over a timescale that is an order of magnitude larger than the timescale of the generation of dislocations by a Frank–Read mechanism. Relaxation is never complete but a residual stress of 10 to 40% remains.
- The efficiency of stress relaxation strongly depends on grain size and density of dislocation sources, in way these factors affect hardening, with smaller grains being harder.
- There is an opposite grain size dependence of relaxation which is caused by
  - the grain size dependence of the initial (compressive) stress;
  - the heterogeneity of the initial stress distribution, which decreases with decreasing grain size.

The modeling of the initial stress is limited in, at least, two ways:

- The actual grain size dependence of diffusion of adatoms over the film and into the grain boundaries is currently unsolved. We have studied the two limits: one where the amount of material diffused into all grain boundaries is the same; the other where the total amount of material is divided equally among all boundaries. The real case being in between these two extremes it is clear that there will be a combined effect of inhomogeneity and increased driving force versus finer microstructures being harder. Relaxation behavior and residual intrinsic stress will be dependent on the balance between them. Finding

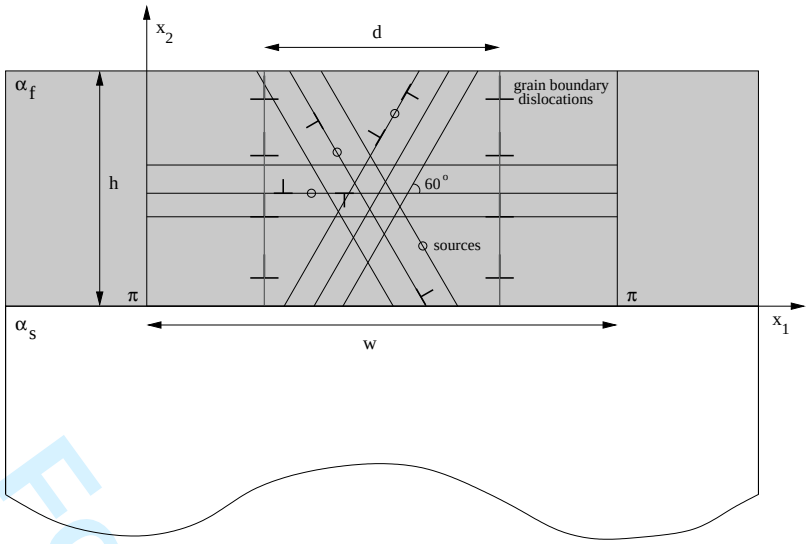

Figure 1. Schematic description of the periodic thin film problem

this balance is the topic of current research.

- In this work, relaxation is assumed to take place after the intrinsic compressive stress has already been formed. This is a simplifying assumption, as in reality the compressive stress is created by grain boundary diffusion at the same time that plasticity by dislocation motion is possible. These two processes are highly uncoupled in terms of timescales since dislocation movement is very much faster than diffusion. This suggests a scenario whereby as soon as the compressive stress reaches the yield strength, some plasticity will occur instantly to relax the stress; followed by continued diffusion and re-activation of plasticity depending on the diffusion rate.

Acknowledgments

This work was supported by the European Commission (6th Framework) through the STREP project NANOMESO.

References

[1] F. A. Floro, S. J. Hearne, J. A. Hunter, P. Kotula, E. Chason, S. C. Seel, C. V. Thompson, Journal of Applied Physics **89** 4886 (2001)
[2] R. Abermann, Vacuum **41** 1279 (1990)
[3] R. W. Hoffman, Thin Solid Films **34** 185 (1976)
[4] L. B. Freund, E. Chason, Journal of Applied Physics **89** 4886 (2001)
[5] M. Laugier, Vacuum **31** 155 (1981)
[6] C. Cammarata, T. M. Trimble, and D. J. Srolovitz, Journal of Materials Research **15** 2468 (2000)
[7] F. Spaepen, Acta Materialia **48** 31 (2000)
[8] C. Friesen and C. V. Thompson, Physical Review Letters. **89** 126103 (2002)
[9] E. Chason, B. W. Sheldon, L. B. Freund, J. A. Floro, S. J. Hearne, Physical Review Letters **88** 156103-4 (2002)
[10] P. R. Guduru, E. Chason, L. B. Freund, Journal of Mechanics and Physics of Solids **51** 2127 (2003)
[11] E. Van der Giessen, A. Needleman, Modelling and Simulation in Materials Science and Engineering **3** 698 (1995)
[12] L. Nicola, E. Van der Giessen, A. Needleman, Journal of Applied Physics **3** 5920 (2003)
[13] L. Nicola, E. Van der Giessen, A. Needleman, Thin Solid Films **53** 329 (2005)
[14] L. Nicola, Y. Xiang, J. J. Vlassak, E. Van der Giessen, A. Needleman, Journal of the Mechanics and Physics of Solids **54** 2089 (2006)
[15] D. S. Balint, V. S. Deshpande, A. Needleman, E. Van der Giessen, International Journal of Plasticity **in press** (2007)
[16] J. Rice, Mechanics of Materials **6** 317 (1987)
[17] H. Gao, L. Zhang, W. D. Nix, C. V. Thompson, E. Artz, Acta Materiala **47** 2865 (1999)
[18] L. B. Freund, Advances in Applied Mechanics **30** 1 (1993)

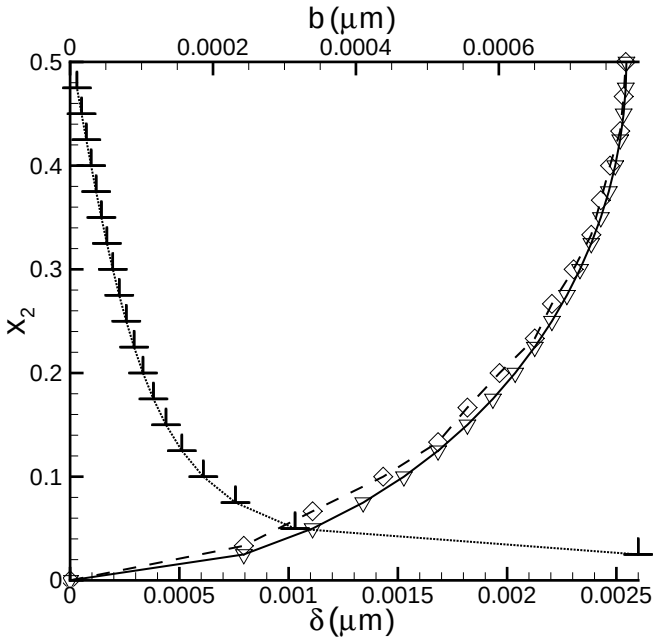

Figure 2. Discretization of grain boundary displacement by dislocations in a film of $h = 0.5\,\mu$m. Solid curve: grain boundary opening δ according to the closed form eq. (2) (for $\delta(h) = 2.6\,$nm) evaluated at dislocation locations indicated by $\bigtriangledown$. Dotted curve: Burgers vector b of the discrete dislocations ($\perp$) computed from the solid curve. Dashed curve: displacements (at nodes indicated by $\diamond$) caused by these discrete dislocations.

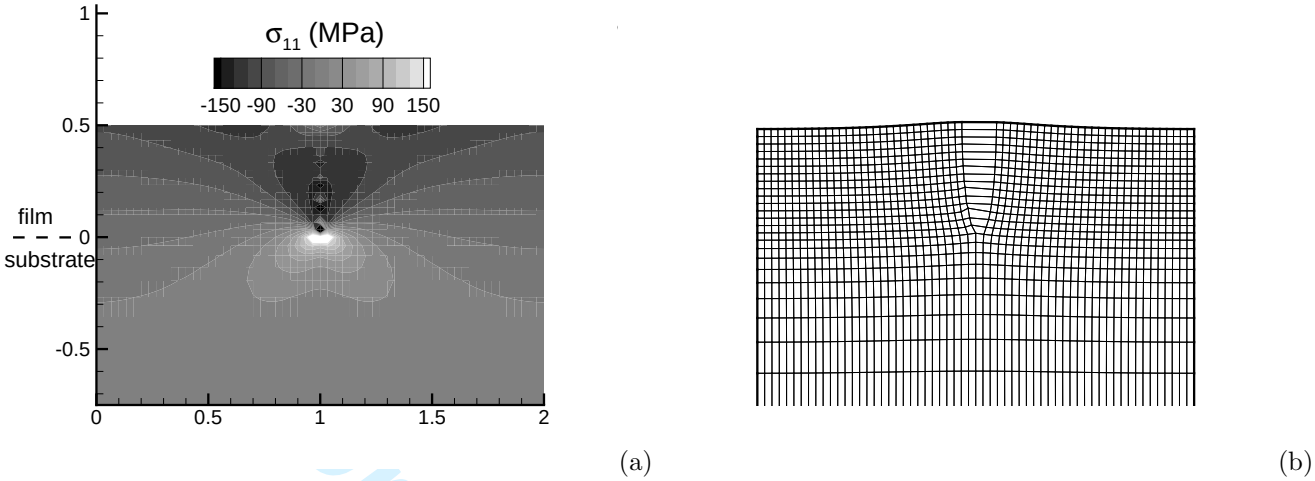

Figure 3. (a) Initial stress σ_{11} and (b) deformed mesh due to grain boundary opening for the film with $d = 2\,\mu$m. Deformations are amplified 50 times.

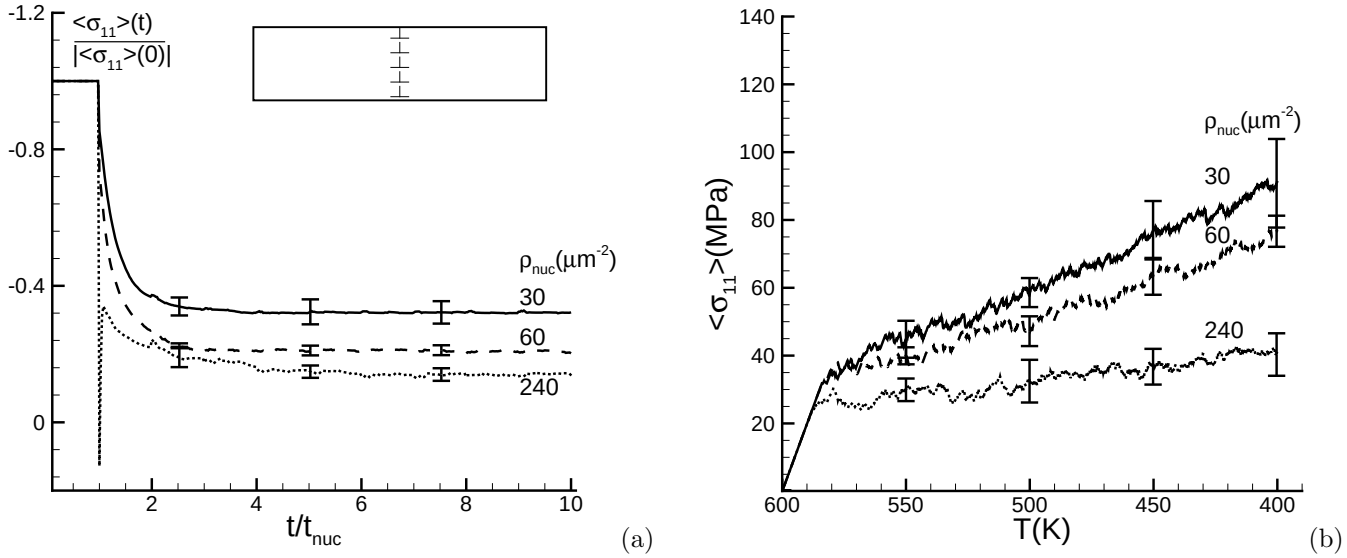

Figure 4. Time-dependent relaxation of intrinsic compressive stress (a) and hardening behavior due to thermal stress (b) in a film with $d = 2\ \mu$m.

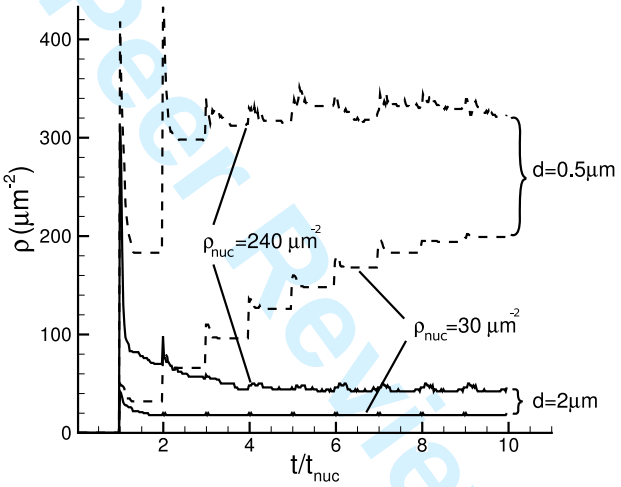

Figure 5. Evolution of dislocation density, ρ, in the course of relaxation for different films and for low vs. high source density.

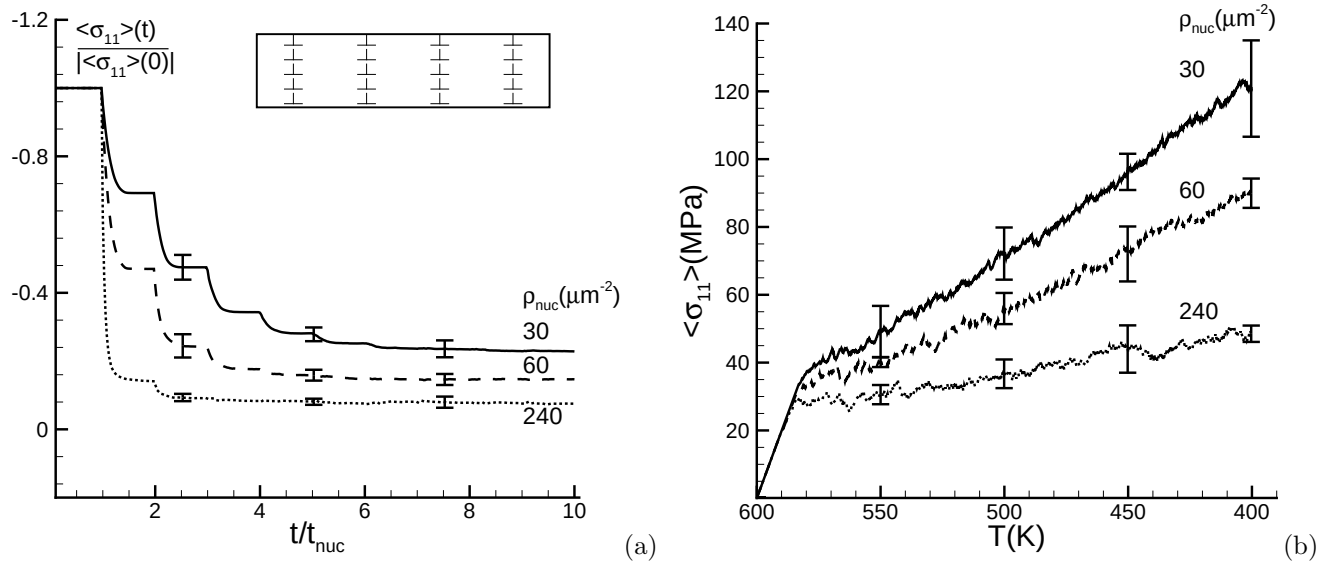

Figure 6. Time-dependent relaxation of intrinsic compressive stress (a) and hardening behavior due to thermal stress (b) in a film with $d = 0.5\,\mu$m.

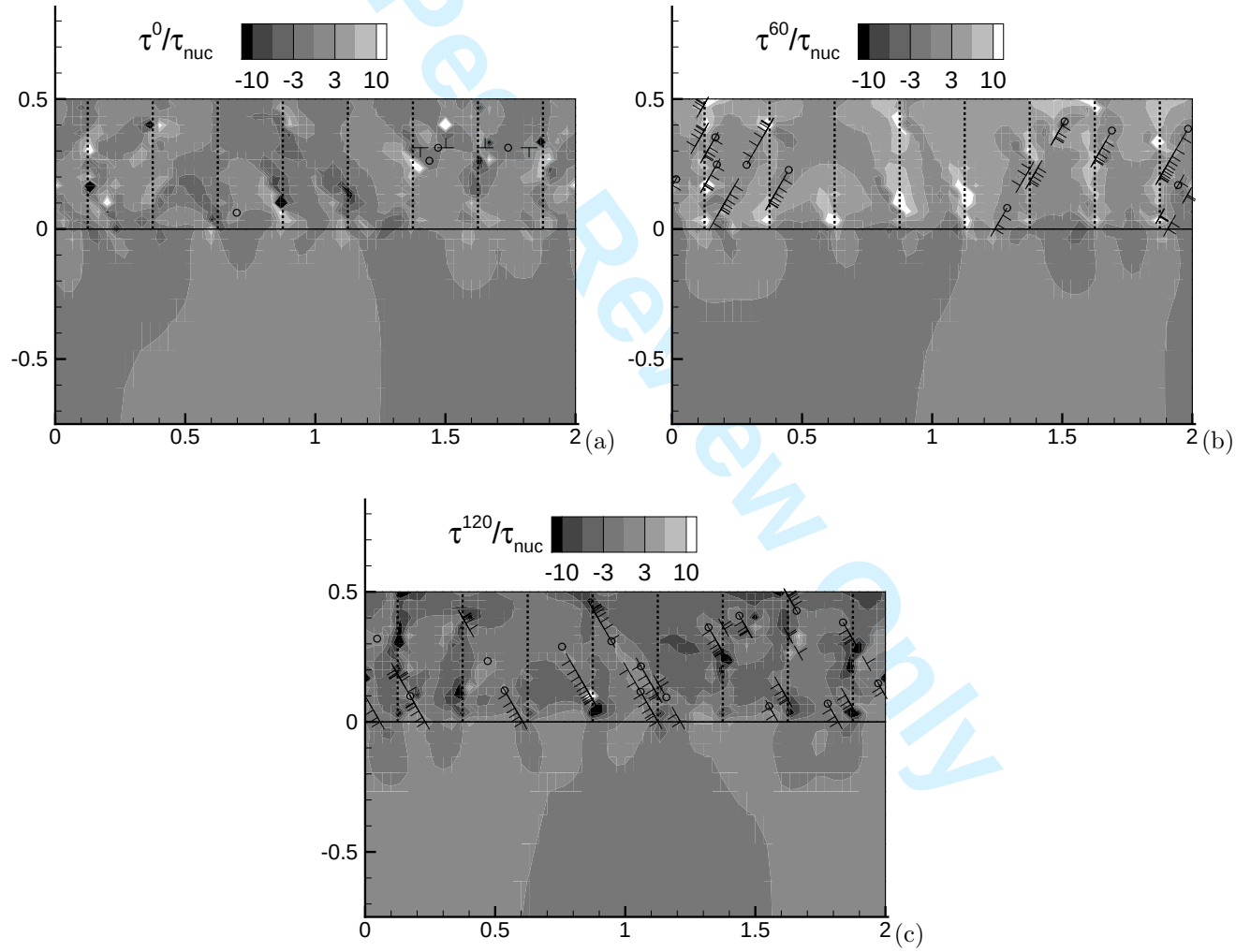

Figure 7. Resolved shear stress τ^{ϕ} at the end of relaxation for $d = 0.25\,\mu$m and $\rho_{\rm nuc} = 30\,\mu{\rm m}^{-2}$ on all slip systems: (a) $\phi = 0°$, (b) $\phi = 60°$ and (c) $\phi = 120°$. The current dislocation (denoted by $\perp$'s) and source (denoted by $\circ$'s) structure for each slip system is superimposed. Stress is normalized with the average nucleation strength $\tau_{\rm nuc}$.

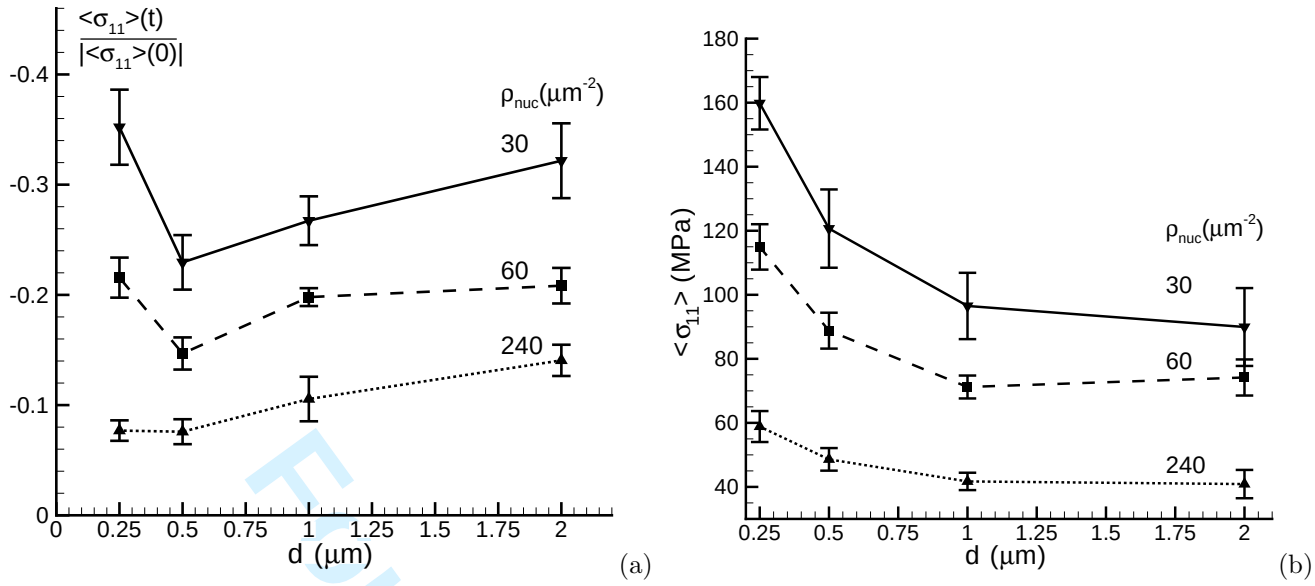

Figure 8. Grain size dependence of the relaxation of intrinsic compressive stress (a) and the hardening behavior due to thermal stress (b) in films with various source densities. The amount of diffusion-inserted material along the grain boundary is constant for all microstructures. The straight lines between datapoints serve merely as guides to the eye.

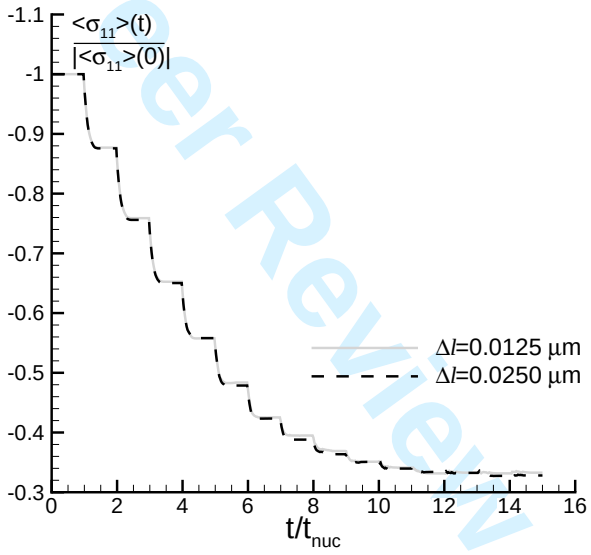

Figure 9. Time-dependent stress relaxation at the default spacing of $\Delta l = 0.025\ \mu$m between the grain boundary dislocations versus that of a finer distribution, $\Delta l = 0.0125\ \mu$m. The grains, with a width of $d = 0.25\ \mu$m, have boundaries of the same width, cf. figure 4a and 6a, and have a source density of $\rho_{\mathrm{nuc}} = 30\ \mu\mathrm{m}^{-2}$.

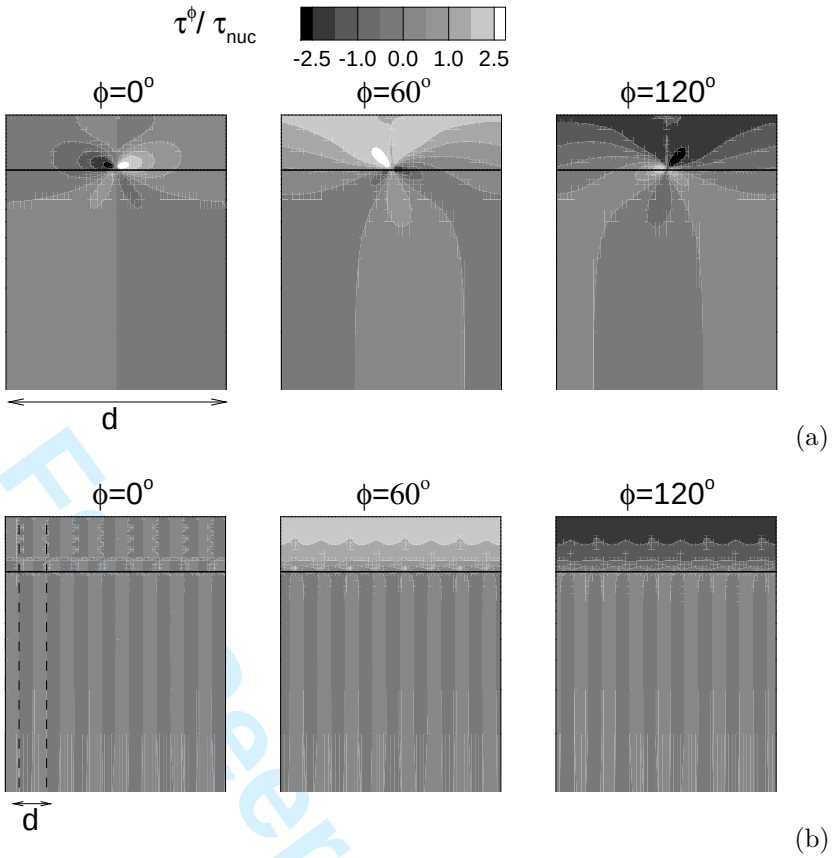

Figure 10. Initial resolved shear stress in three slip systems $d = 2\,\mu$m (a) and $d = 0.25\,\mu$m (b). The total amount of diffusion-inserted material along the grain boundaries is the same for both cases.

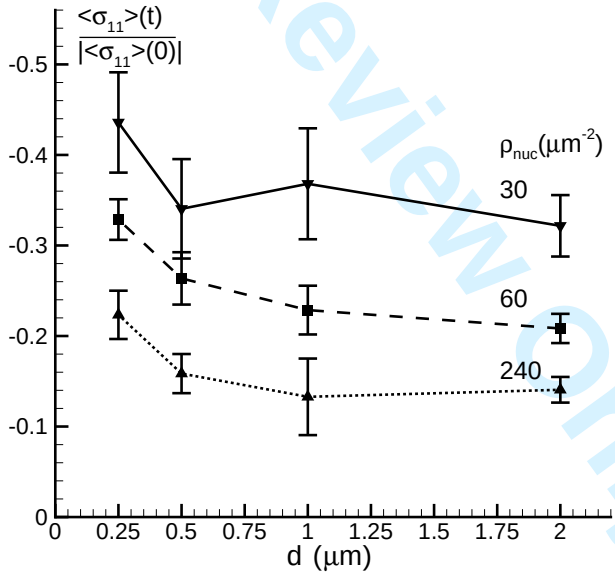

Figure 11. Grain size dependence of the relaxation of intrinsic compressive stress (a) and the hardening behavior due to thermal stress (b) in films with various source densities. Contrary to figure 8, the total amount of diffusion-inserted grain boundary material is constant, i.e. $\delta(h)/d$ is constant. The straight lines between datapoints serve merely as guides to the eye.

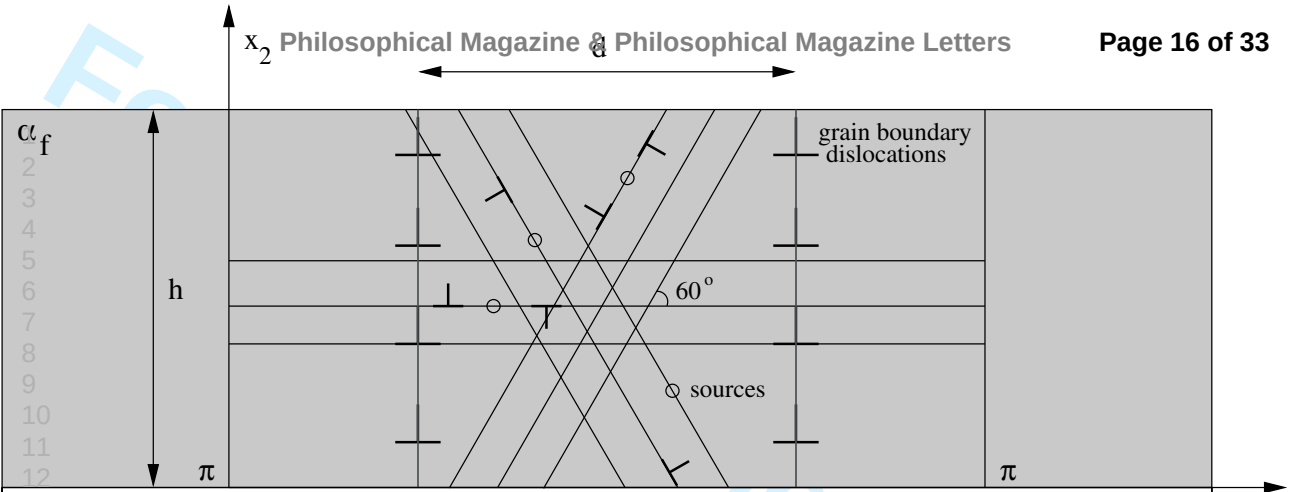

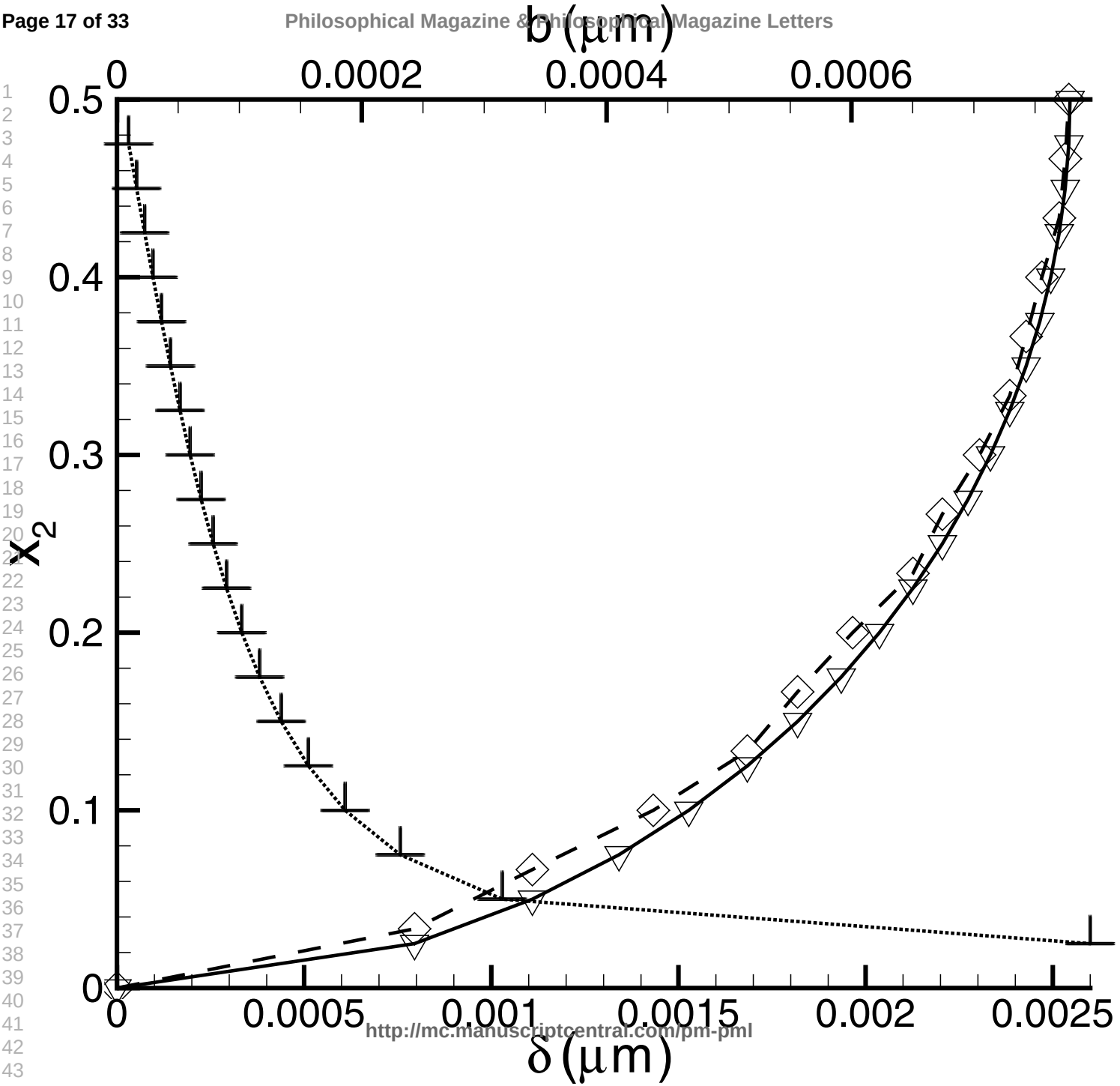
b (μm)
0
0.0002
0.0004
0.0006
0.5
0.4
0.3
0.2
0.1
0
x_2
0
0.0005
0.001
0.0015
0.002
0.0025
δ (μm)

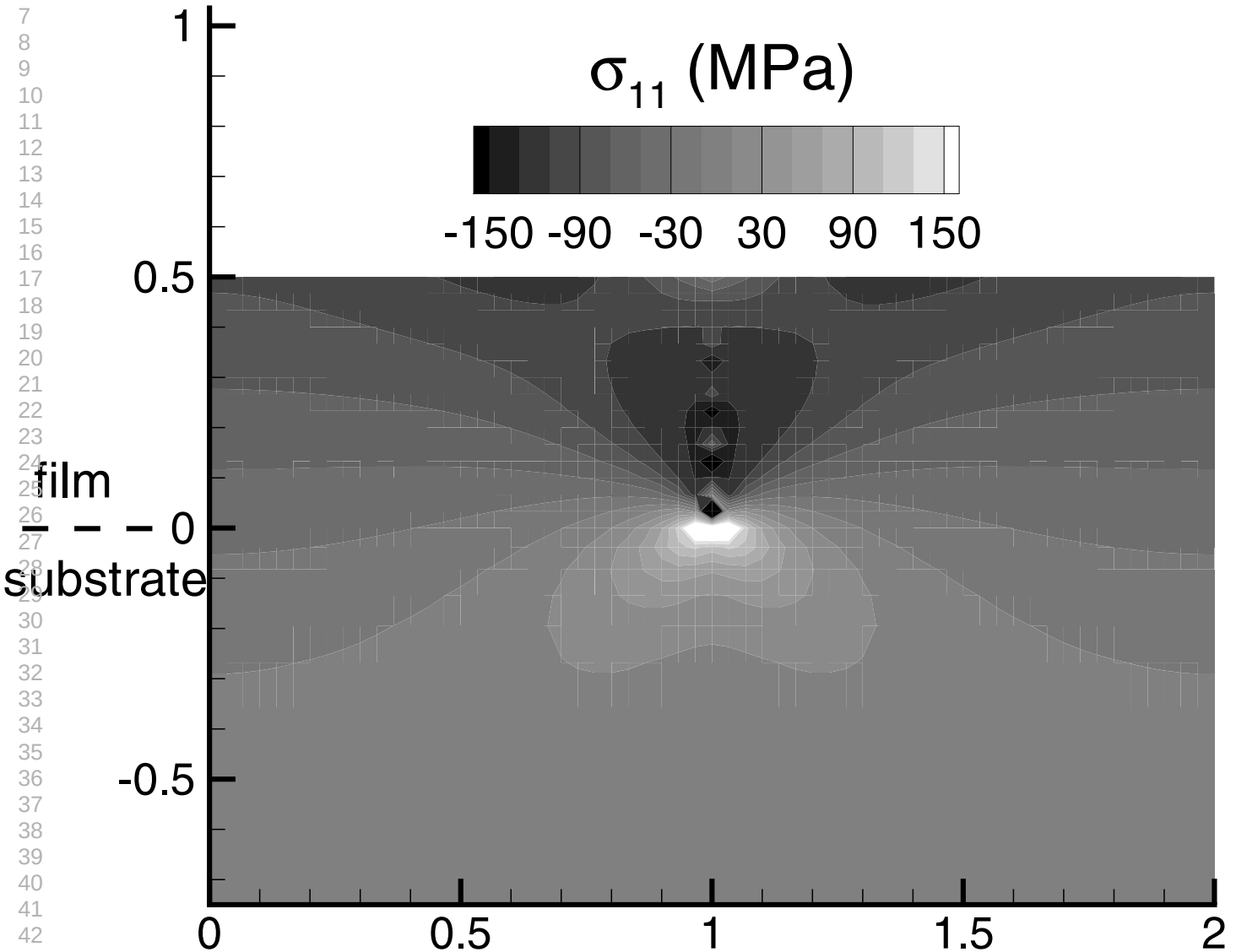
σ11 (MPa)
-150 -90 -30 30 90 150
1
0.5
0
-0.5
film
substrate
0
0.5
1
1.5
2

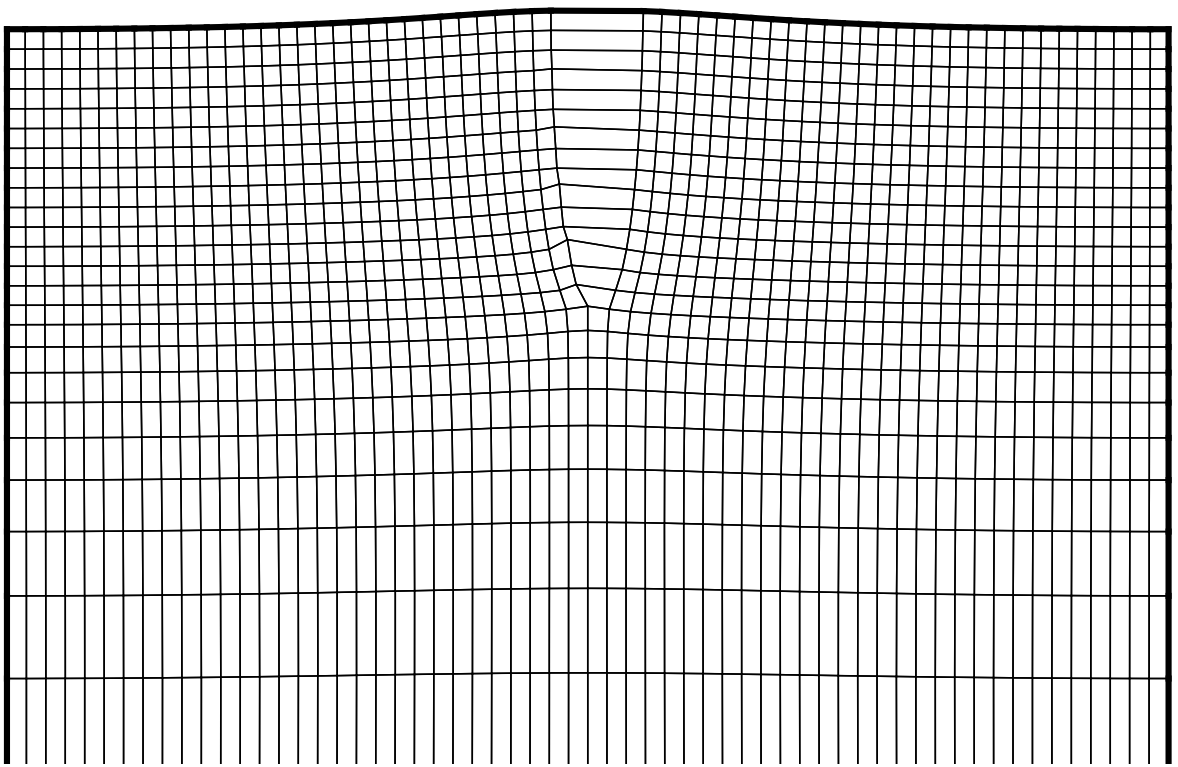

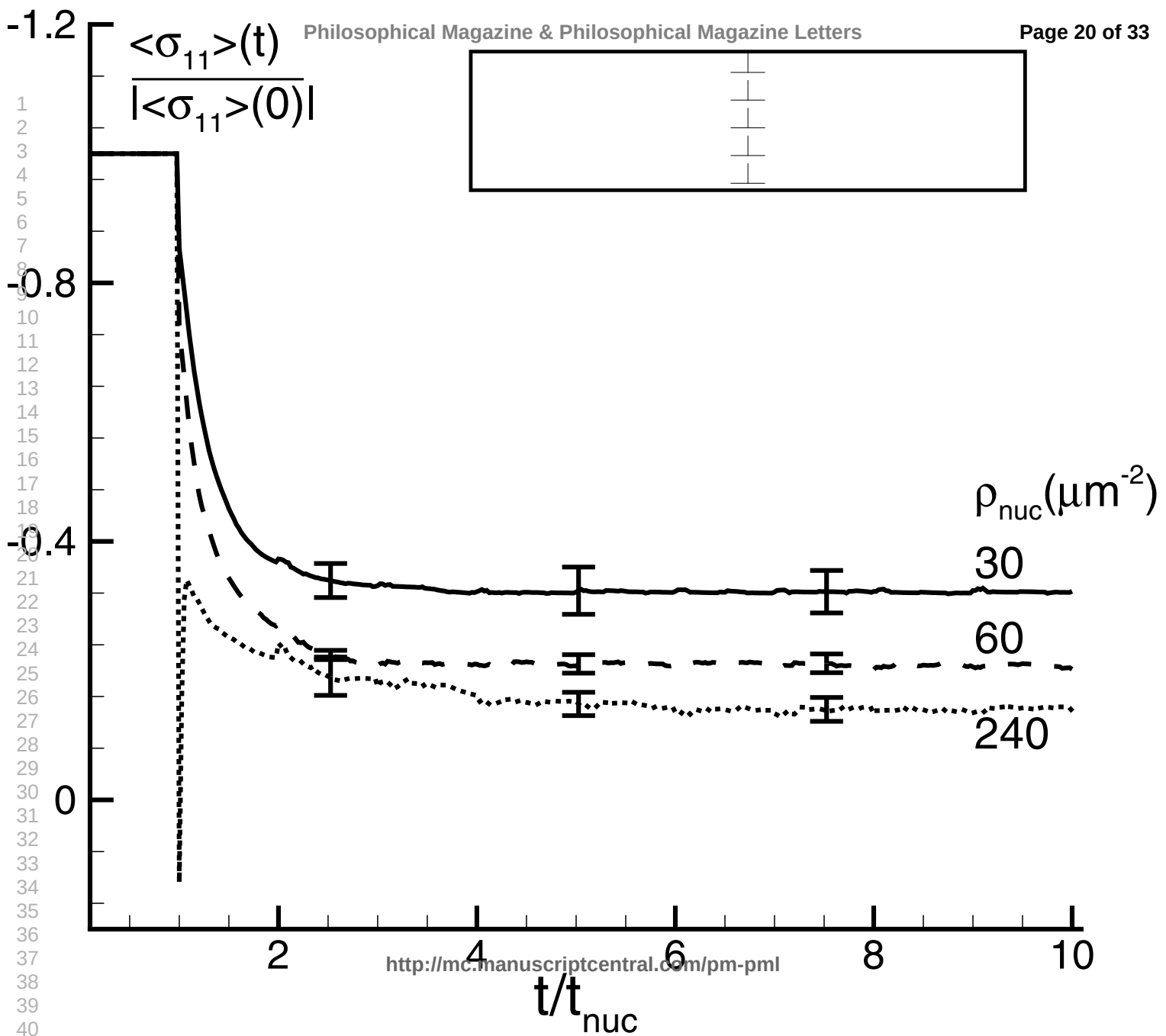
-1.2
-0.8
-0.4
0
2
4
6
8
10
$\frac{<\sigma_{11}>(t)}{|<\sigma_{11}>(0)|}$
$\rho_{nuc}(\mu m^{-2})$
30
60
240
t/t_{nuc}

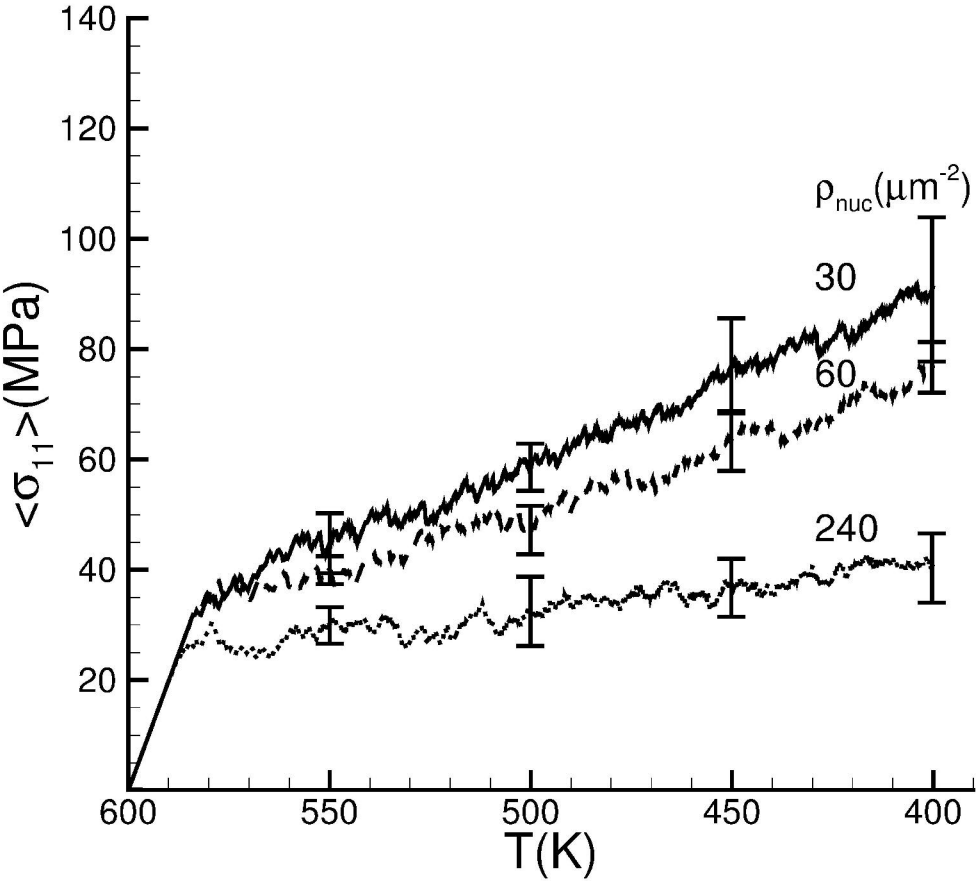

203x184mm (600 x 600 DPI)

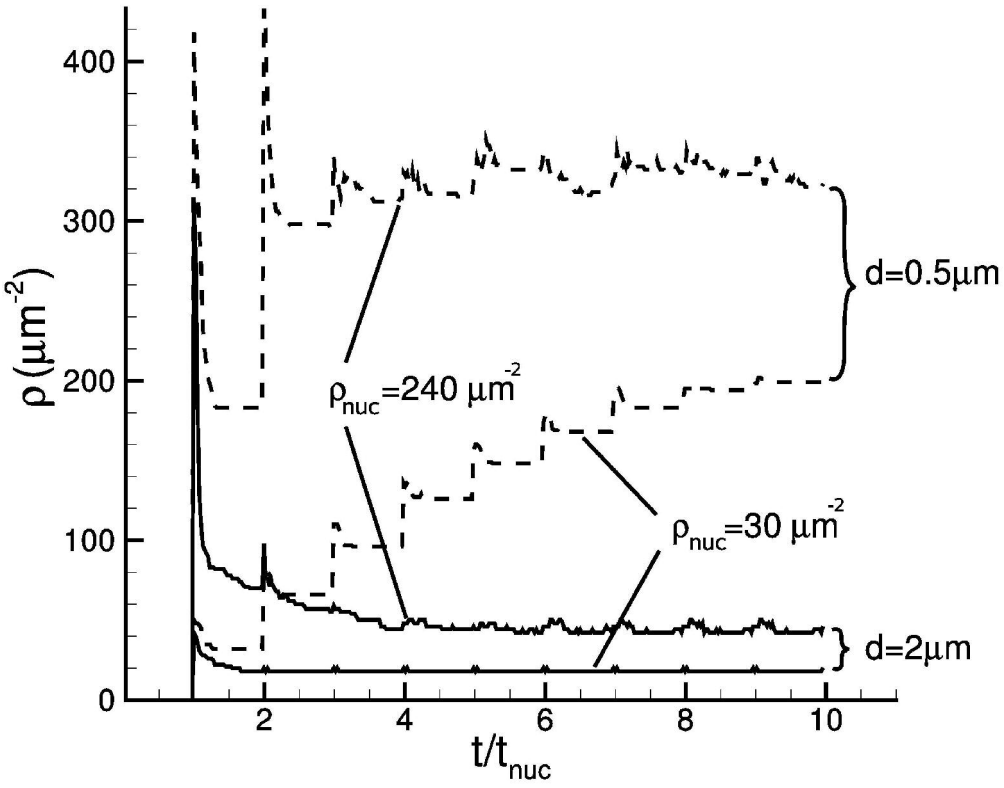

116x93mm (600 x 600 DPI)

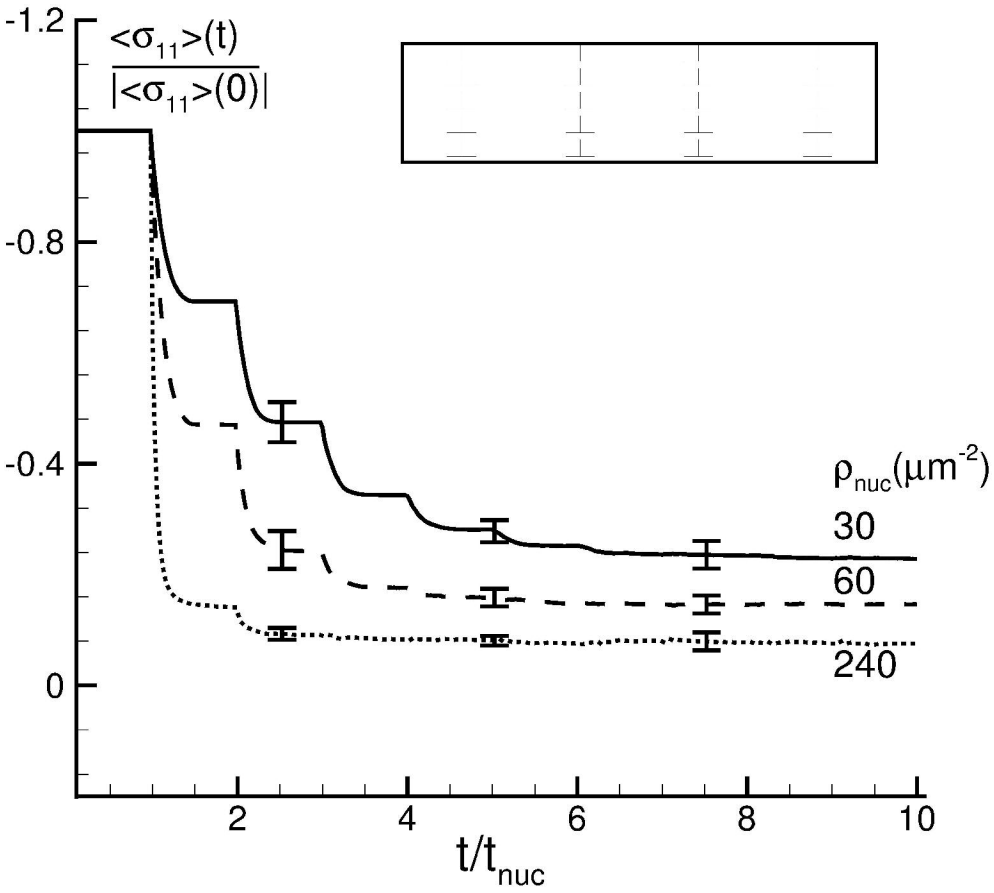

202x179mm (600 x 600 DPI)

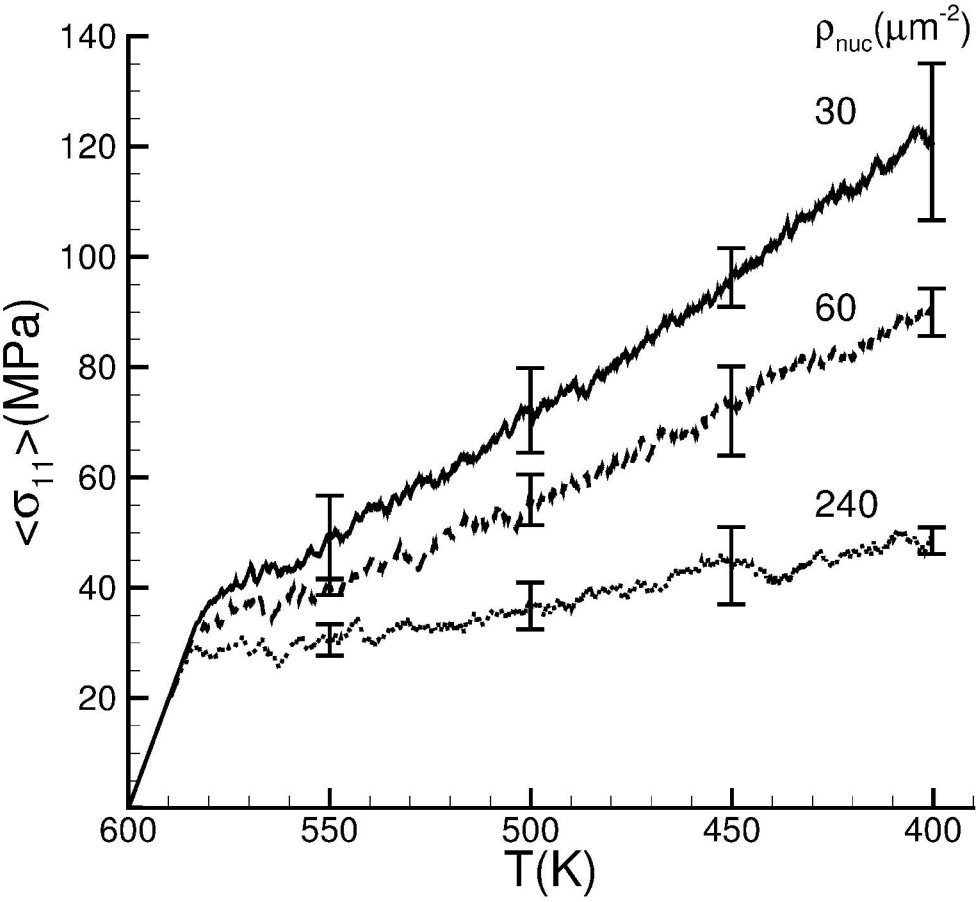

203x184mm (600 x 600 DPI)

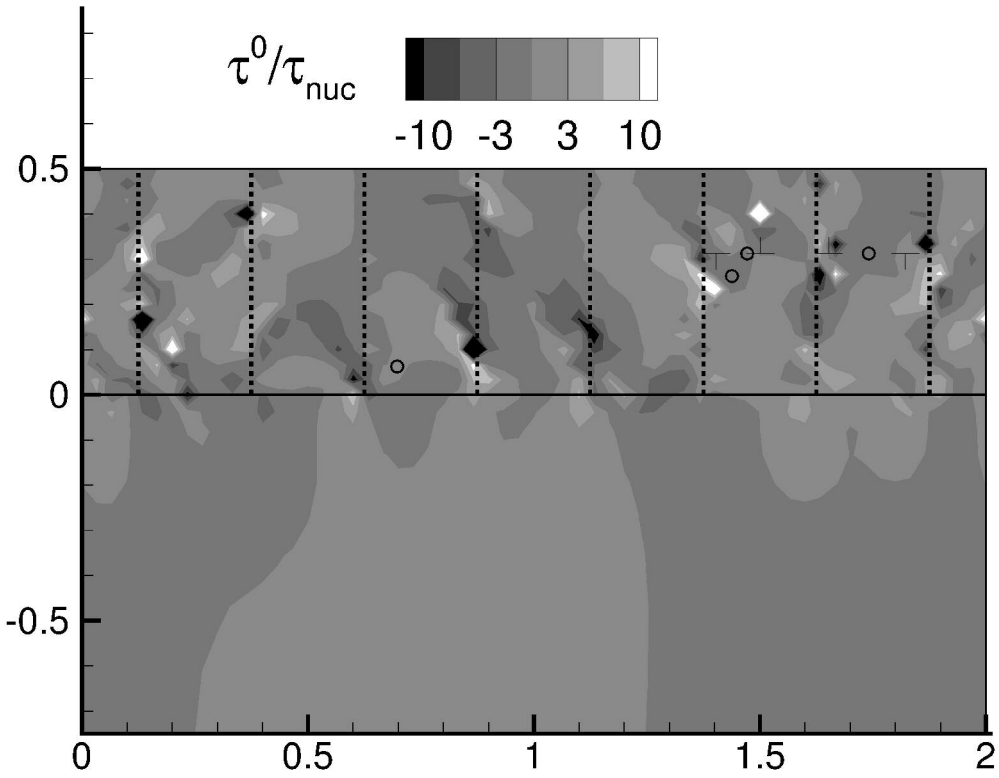

189x148mm (600 x 600 DPI)

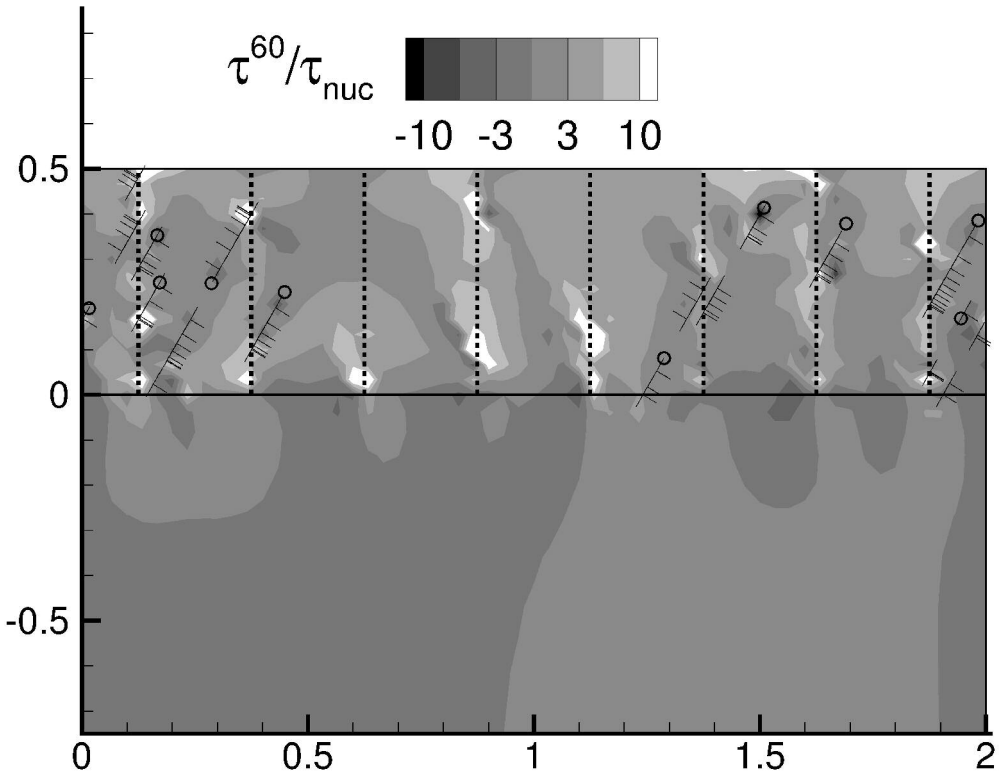

189x148mm (600 x 600 DPI)

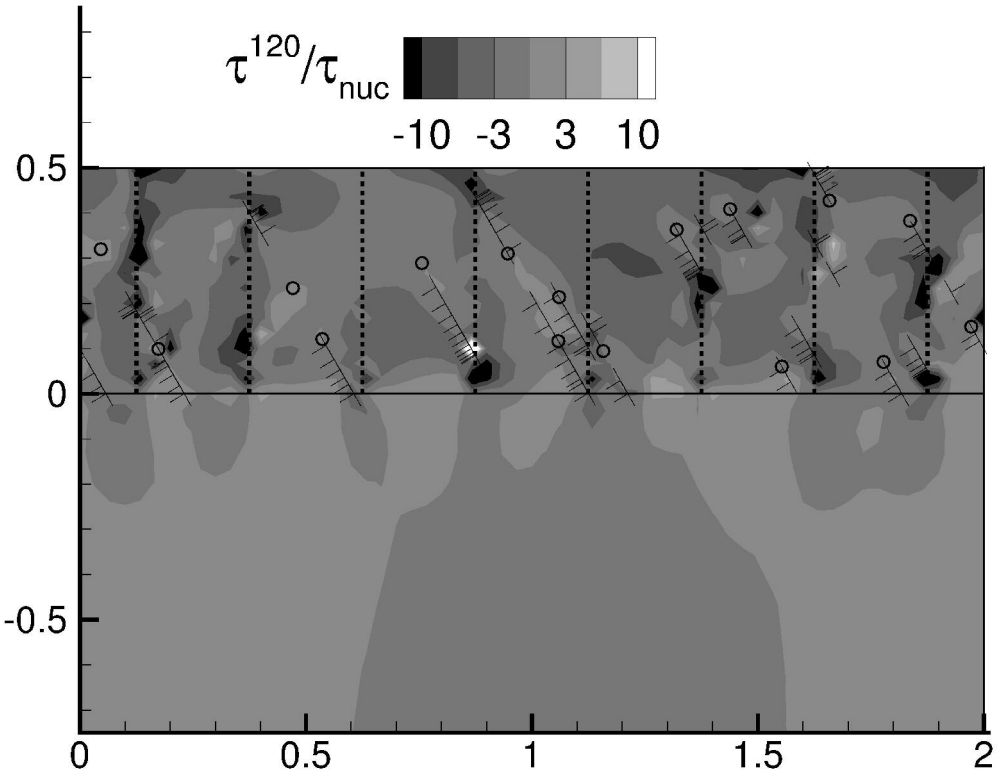

189x158mm (600 x 600 DPI)

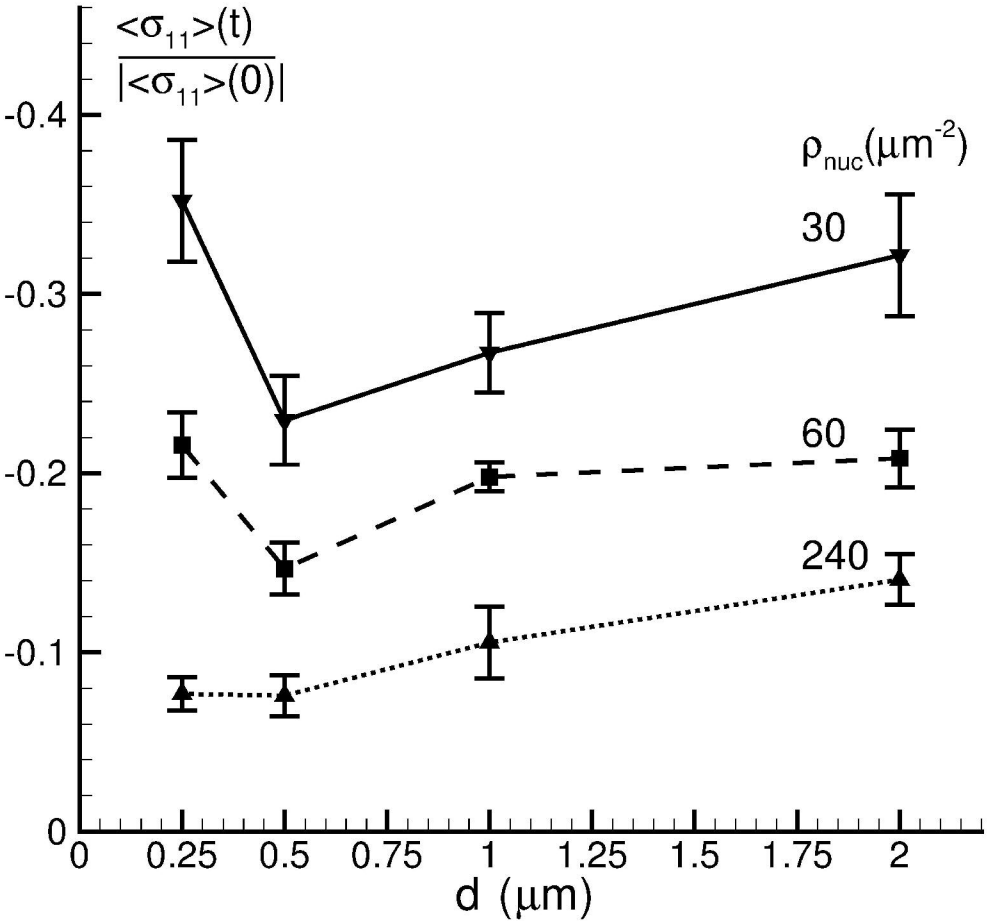

190x178mm (600 x 600 DPI)

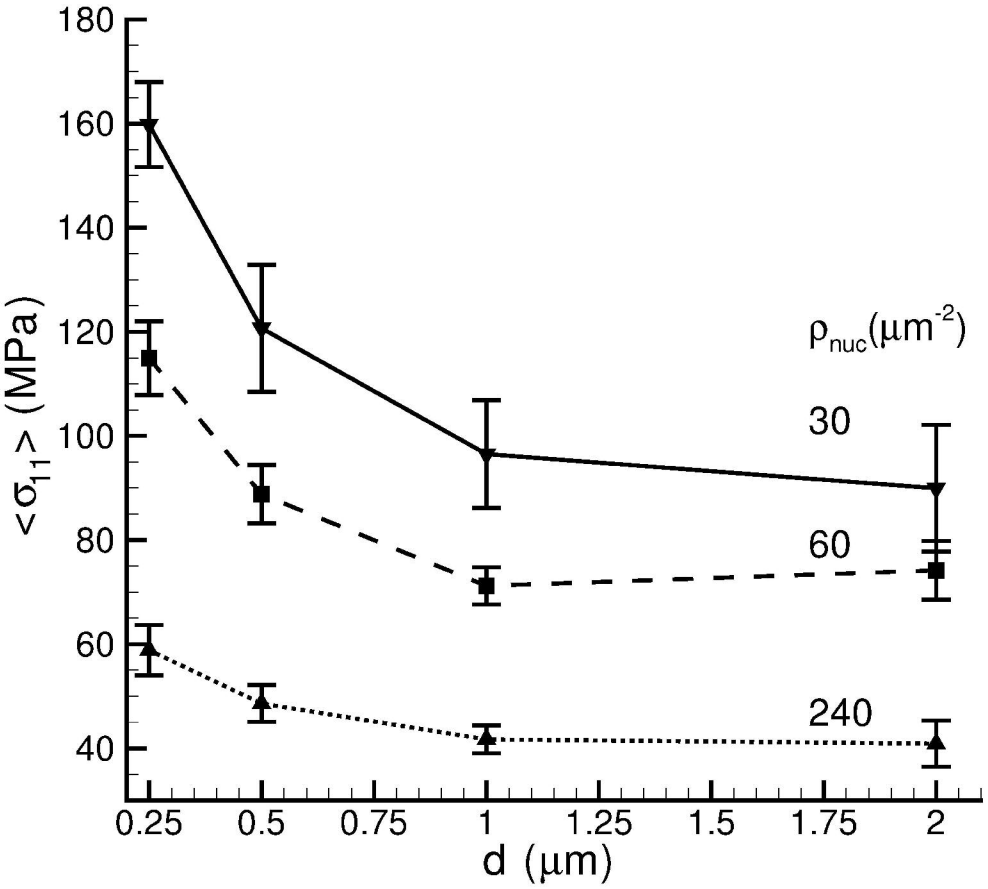

201x178mm (600 x 600 DPI)

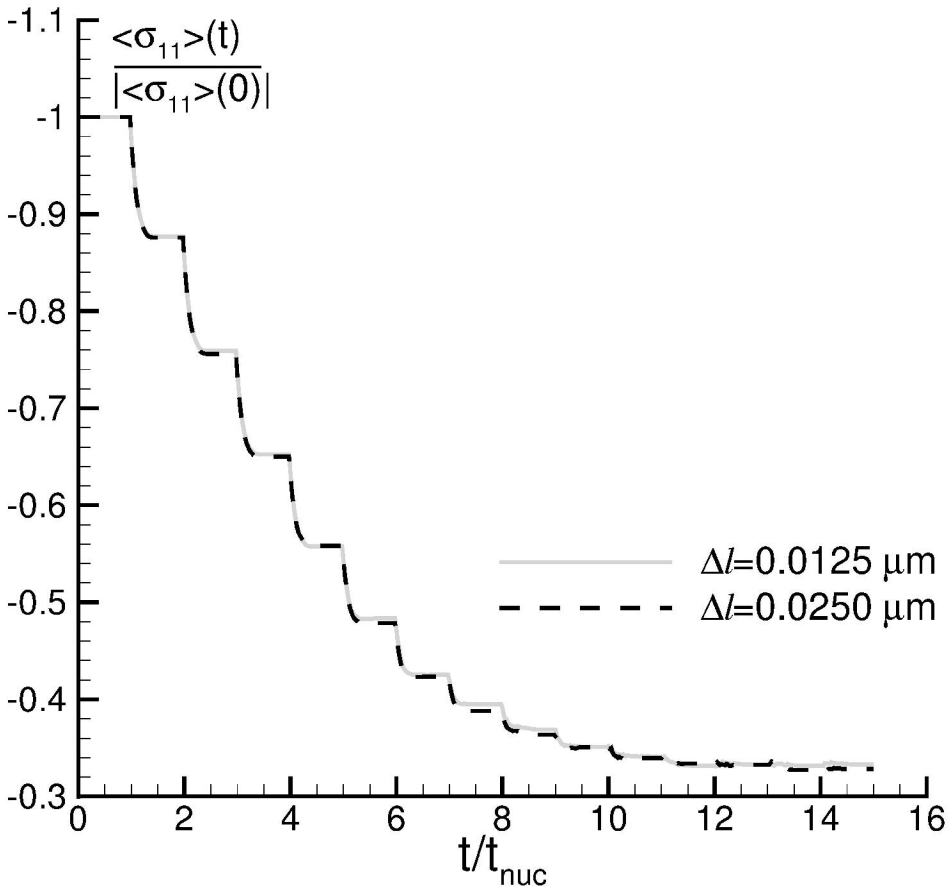

202x179mm (600 x 600 DPI)

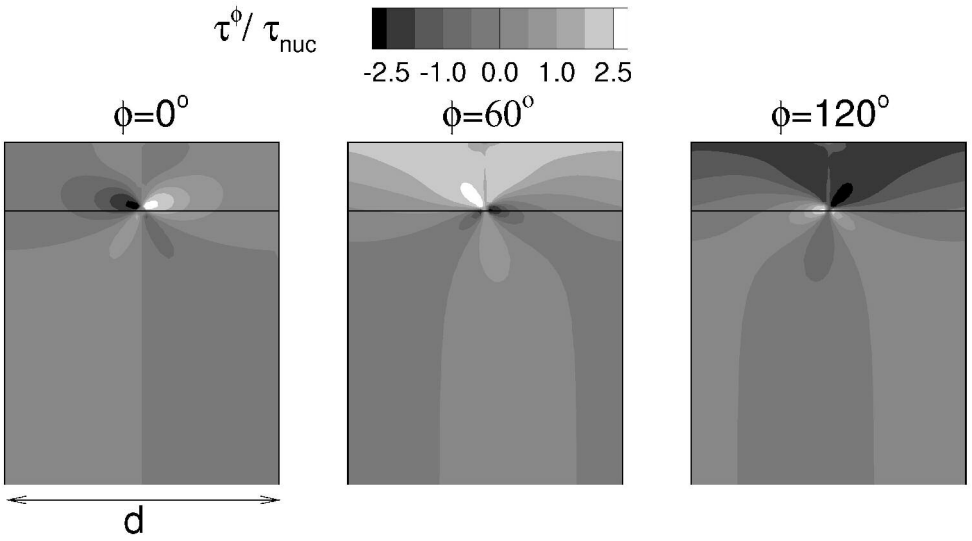

167x94mm (600 x 600 DPI)

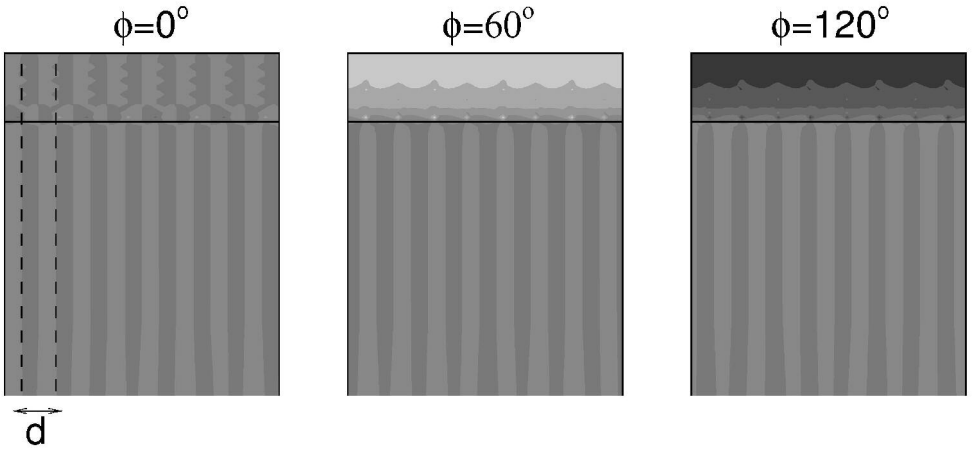

167x81mm (600 x 600 DPI)

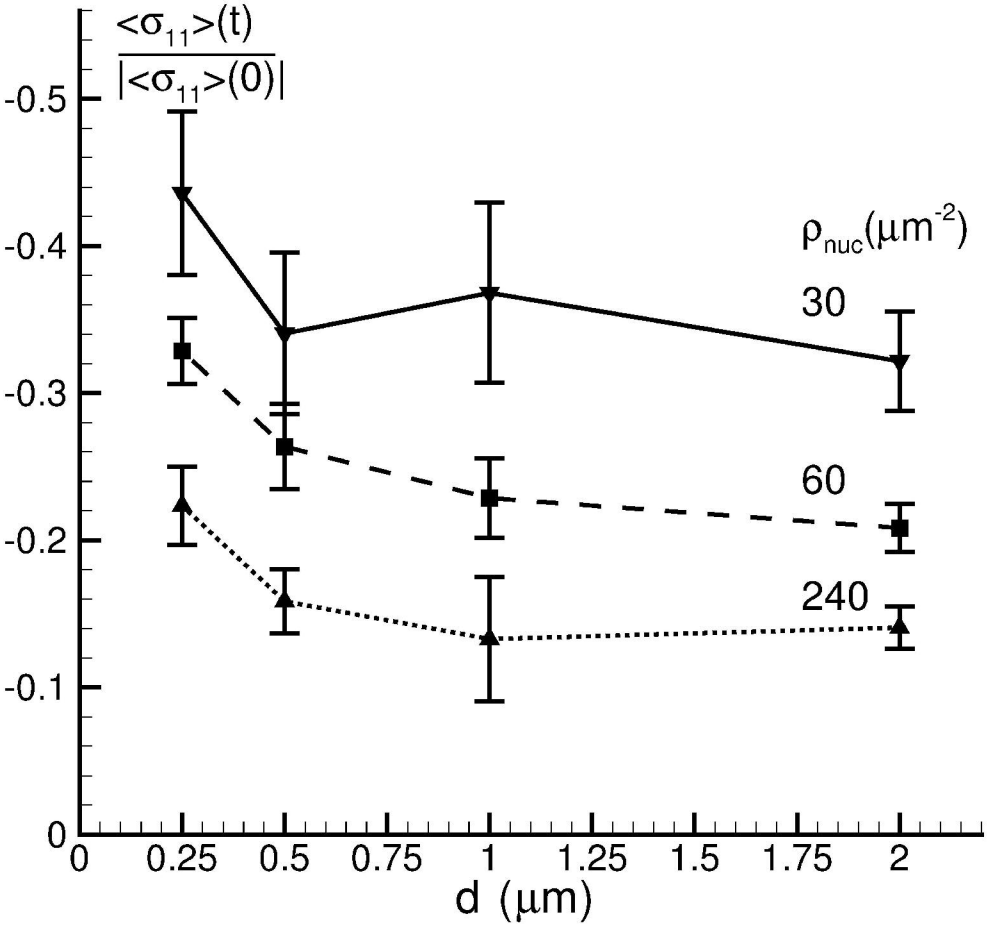

190x178mm (600 x 600 DPI)